frontiers in Microbiology

ORIGINAL RESEARCH
published: 13 January 2021
doi: 10.3389/fmicb.2020.612239

Analysis of Cell–Cell Bridges in *Haloferax volcanii* Using Electron Cryo-Tomography Reveal a Continuous Cytoplasm and S-Layer

*Shamphavi Sivabalasarma[1,2], Hanna Wetzel[1], Phillip Nußbaum[1], Chris van der Does[1], Morgan Beeby[3] and Sonja-Verena Albers[1,2]**

[1] Molecular Biology of Archaea, Institute of Biology II, Faculty of Biology, University of Freiburg, Freiburg, Germany, [2] Spemann Graduate School of Biology and Medicine, University of Freiburg, Freiburg, Germany, [3] Department of Life Sciences, Imperial College London, London, United Kingdom

Halophilic archaea have been proposed to exchange DNA and proteins using a fusion-based mating mechanism. Scanning electron microscopy previously suggested that mating involves an intermediate state, where cells are connected by an intercellular bridge. To better understand this process, we used electron cryo-tomography (cryoET) and fluorescence microscopy to visualize cells forming these intercellular bridges. CryoET showed that the observed bridges were enveloped by an surface layer (S-layer) and connected mating cells via a continuous cytoplasm. Macromolecular complexes like ribosomes and unknown thin filamentous helical structures were visualized in the cytoplasm inside the bridges, demonstrating that these bridges can facilitate exchange of cellular components. We followed formation of a cell–cell bridge by fluorescence time-lapse microscopy between cells at a distance of 1.5 μm. These results shed light on the process of haloarchaeal mating and highlight further mechanistic questions.

Keywords: ***Haloferax volcanii*, electron cryo-tomography, archaea, horizontal gene transfer, cell fusion, cell fusion, fluorescence microscopy**

OPEN ACCESS

Edited by:
John A. Fuerst, The University of Queensland, Australia

Reviewed by:
Aharon Oren, Hebrew University of Jerusalem, Israel
Reinhard Rachel, University of Regensburg, Germany

***Correspondence:**
Sonja-Verena Albers
sonja.albers@biologie.uni-freiburg.de

Specialty section:
This article was submitted to Biology of Archaea, a section of the journal Frontiers in Microbiology

Received: *30 September 2020*
Accepted: *11 December 2020*
Published: *13 January 2021*

Citation:
Sivabalasarma S, Wetzel H, Nußbaum P, van der Does C, Beeby M and Albers S-V (2021) Analysis of Cell–Cell Bridges in Haloferax volcanii Using Electron Cryo-Tomography Reveal a Continuous Cytoplasm and S-Layer. Front. Microbiol. 11:612239. doi: 10.3389/fmicb.2020.612239

INTRODUCTION

Horizontal gene transfer is fundamental to archaeal and bacterial evolution. The diverse mechanisms of horizontal transfer, however, remain incompletely understood (Wagner et al., 2017). These mechanisms include uptake of DNA via natural transformation, transfer of conjugative plasmids, transduction, uptake of DNA via membrane vesicles and cell fusion hybrids (Wagner et al., 2017). Members of Euryarchaeota, *Pyrococcus furiosus*, and *Thermococcus kodakaraensis* are naturally competent taking up linear and circular DNA (Sato et al., 2005; Lipscomb et al., 2011). Transfer of conjugative plasmids was described first in *Sulfolobales* by the isolation of the first archaeal conjugative plasmid in 1995 (Schleper et al., 1995; Prangishvili et al., 1998; Stedman et al., 2000). Interestingly, analysis of the genome of *Sulfolobales* revealed the insertion of proviral DNA from *Sulfolobus* spindle-shaped virus 1 (SSV1) (Schleper et al., 1992). SSV1 stays integrated in archaeal genomes and produce viral particles budding from the cells for the transfer of viral DNA (Quemin et al., 2016). Also haloarchaeal viruses have been shown to drive the genetic variation

of different haloarchaeal species (Cuadros-Orellana et al., 2007; Tschitschko et al., 2018; Mizuno et al., 2019).

Methanococcus voltae PS produces viral particles named "voltae transfer agent" (VTA) which can carry chromosomal fragments instead of viral DNA (Bertani, 1999; Eiserling et al., 1999; Lang et al., 2012). Similarly to VTA, *Thermococcales* release membrane vesicles packed with chromosomal and plasmid DNA for the exchange of genetic material (Soler et al., 2008). Members of *Sulfolobus* spp. can exchange DNA upon UV-induced DNA damage allowing for DNA repair using homologous recombination (Fröls et al., 2008; Ajon et al., 2011). Cell aggregates are formed mediated by UV-induced pili (Ups-pili) and the crenarchaeal exchange of DNA system (Ced-system) is activated (Fröls et al., 2008, 2009; Ajon et al., 2011). Using the Ups-pili cell–cell contact is established and DNA is exchanged (Van Wolferen et al., 2016). Remarkably the exchange is species-specific possibly being mediated by the degree of N-glycosylation of Ups-pili (van Wolferen et al., 2020). Finally bidirectional gene transfer occurs in haloarchaea via cell fusion (Mevarech and Werczberger, 1985; Rosenshine et al., 1989).

Here, the cell biological prerequisites for the previously observed DNA transfer through cell fusion in haloarchaea are elucidated. In the 1980s, it was described that mixing of two different auxotrophic strains of the halophilic euryarchaeon *Haloferax volcanii*, resulted in prototrophic recombinant cells. The mating frequency was determined in the presence of DNase to rule out natural transformation and was 10^{-6} (Mevarech and Werczberger, 1985). It was proposed that transfer of genetic material occurred via an uncharacterized fusion-based mating mechanism (Mevarech and Werczberger, 1985). Remarkably, the transfer of DNA in *H. volcanii* is bidirectional without a specific donor or recipient and since mating and subsequent DNA exchange has been observed within the two species *H. volcanii* and *H*aloferax *mediterranei*, it is not necessarily species specific (Naor et al., 2012). It was observed that two *H. volcanii* cells can fuse to form a hybrid state (Naor et al., 2012; Naor and Gophna, 2013). In this state, large chromosomal DNA fragments are exchanged and after recombination followed by cell separation, this results in genetic hybrids of the parents (Naor et al., 2012; Naor and Gophna, 2013). CRISPR spacers matching chromosomal genes, including housekeeping genes, are also exchanged between species (Turgeman-Grott et al., 2019). Strikingly, mating frequency depends on factors that impact the cell surface such as external salt concentration and N-glycosylation of the surface layer (S-layer) (Shalev et al., 2017). Defects in the N-glycan of S-layer proteins significantly reduce mating frequencies, suggesting an important role for S-layer glycosylation in initiation of cell–cell interaction and cell fusion (Shalev et al., 2017). Early electron micrographs from 1975 when *H. volcanii* was isolated and characterized as well as other scanning electron micrographs of *H. volcanii* have suggested the formation of intermediate intercellular bridges prior to cell fusion (Mullakhanbhai and Larsen, 1975; Rosenshine et al., 1989). These cell–cell bridges might allow for an exchange of genetic material and drive cell fusion (Naor and Gophna, 2013). Exchange of genetic material has only been observed on solid media in previous studies, prompting questions about the mechanisms involved in mating. Formation of possible cell–cell bridges between cells has also been observed in other archaeal lineages, such as members of *Sulfolobales* (Schleper et al., 1995), *Thermococcales* (Kuwabara et al., 2005), and even between Nanoarchaea and *Thermoplasmatales* (Comolli and Banfield, 2014). Formation of cell–cell bridges was also reported in bacterial species. These nanotubes are enveloped by a membrane layer and build a bridge between two neighboring bacterial cells allowing an exchange of cytoplasm (Dubey and Ben-Yehuda, 2011; Baidya et al., 2018).

To better characterize the mechanism of horizontal gene transfer by fusion in *H. volcanii,* we used electron cryo-tomography (cryoET) to preserve whole cells in a frozen hydrated state. We identified and imaged cell–cell bridges connecting the cytoplasms of pairs of cells grown in liquid media. Tomograms revealed that two mating cells shared a continuous membrane, a continuous S-layer and had continuous connected cytosols. Strikingly, macromolecular structures were detected in the cell–cell bridges likely to be ribosomes. Fluorescence time-lapse microscopy of *H. volcanii* cells with fluorescently stained S-layers showed how cells established an intercellular bridge as an intermediate state prior to cell fusion.

MATERIALS AND METHODS

Strains and Growth Conditions

Growth of *H. volcanii* H26 and RE25 was performed as described previously (Allers et al., 2004; Esquivel and Pohlschroder, 2014; Duggin et al., 2015). The cells were grown in Hv-YPC medium containing 2.4 M NaCl, 0.17 M of $MgSO_4 \times 7\ H_2O$, 0.27 M $MgCl_2 \times 6\ H_20$, 0.05 M KCl, 3 mM $CaCl_2$ and 12 mM TRIS, HCL (pH 7.5) with 0.5% (wt/vol) yeast extract (Difco), 0.1% (wt/vol) peptone (Oxoid), and 0.5% (wt/vol) casamino acids (Bacto). Selective Casamino acid medium (CA medium) was prepared as Hv-YPC medium but yeast extract and peptone were omitted. CAB medium was prepared as CA medium and contained a 100× fold diluted expanded trace element solution, containing 5 g/L ethylenediaminetetraacetic acid (EDTA), 0.8 g/L $FeCl_3$, 0.05 g/L $ZnCl_2$, 0.01 g/L $CuCl_2$, 0.01 g/L $CoCl_2$, 0.01 g/L H_3BO_3, 1.6 g/L $MnCl_2$, 0.01 g/L Ni_2SO_4, and 0.01 g/L H_2MoO_4. The pH was adjusted to pH 7.0 with NaOH and the solution was filter sterilized.

Electron Cryo-Tomography

Haloferax volcanii RE 25 was inoculated in 5 mL CA medium supplemented with 1 g/l thiamine and 0.1 μg/L biotin, 10 μg/mL uracil and 50 μg/mL tryptophan that was incubated at 42°C overnight. A total of 5 and 15 μL of the pre-culture was inoculated in 20 mL CA medium and incubated again at 42°C overnight. At OD_{600} of 0.05, the cells were harvested at 2,000 × *g* for 20 min at 40°C. The pellet was dissolved in 1 mL CA medium and again pelleted at 2,000 × *g* for 10 min at 40°C. The cell pellet was dissolved again in CA medium to a theoretical OD_{600} of 3 or 5. The cells were mixed with BSA-coated 10 nm gold

fiducial markers and 2.5 μL of cells were applied to a freshly glow-discharged copper Quantifoil R2/2 grid (300 mesh). The vitrification of the grid was done using the Vitrobot Mark IV (FEI). The grid was blotted on the back using a repellent Teflon membrane and subsequently plunge-frozen in liquid ethane. Electron cryotomography was conducted with a 200 kV Twin FEI F20 (FEG) equipped with a Falcon II direct electron detector. The software package Leginon was used to record tilt series (Carragher et al., 2000). A total cumulative electron dose of 120 e-/Å^2 was used per tilt series with −3 to −6 μm defocus. The tomograms were collected bidirectionally in a tilt range of ±54° starting at +24°collecting through – 54° and then the remaining tilts with 3° increments and a pixel size of 8.28 Å. Tomograms were reconstructed automatically using RAPTOR software and IMOD (Kremer et al., 1996; Mastronarde, 1997; Amat et al., 2008).

S-Layer Staining

Haloferax volcanii H26 was inoculated in 5 mL CAB medium supplemented with 10 μg/mL uracil and grown overnight at 45°C. A total of 220 μL were inoculated in 20 mL of the main culture which was grown overnight at 45°C. The cells were harvested at OD_{600} = 0.2 at 1,800 × *g* for 10 min at 25°C. The pellet was resuspended in 2 mL of buffered media and washed three times at 3,400 × g for 10 min at RT and resuspended in 500 μL buffered media. The pH was adjusted to pH 8–8.5 with 1 M $NaHCO_3$ and 50 μg of Alexa Fluor 488 NHS Ester (Thermo Fisher Scientific) was added. The cells were incubated at RT for 1 h while rotating. To remove excess dye, the cells were washed three times as above with 500 μL CAB medium.

Isolation of Stained S-Layer

Staining was checked by sonicating the cells for 10 min in an ultrasonic bath. Afterwards, the cell debris was pelleted at 3,400 × *g* for 10 min at RT. SDS was added to a final concentration of 0.01% and the mixture was centrifuged again at 3,400 × *g* for 10 min at RT. The supernatant was divided into 2 × 500 μL and centrifuged at 190,000 × *g* for 1 h at 4°C. The resulting pellets were resuspended in 50 μl 1× loading dye and in 5 μL 1× PBS, 0.1% Triton-X 100. Both pellets were incubated at 6°C, in a light-protected manner for 48 h and then mixed together. This was incubated for 2 1/2 h at 37°C and 10 μL was used for an SDS-PAGE and detection of the fluorescence signal.

S-Layer Isolation

For S-layer isolation, 400 mL of H26 was grown at 45°C to an OD_{600} of 1.37. The cells were pelleted at 6,200 × *g* for 25 min at 4°C. The pellet was resuspended in 200 mL CA medium and 60 mL of 0.5 M EDTA (pH 6.7) was added. Subsequently, the pellet was incubated at 37°C while shaking for 30 min. The spheroplasts were removed via centrifugation in an iterative manner at 3,000 × *g* for 15 min, 7,000 × *g* for 5 min and 13,000 × *g* for 10 min. The supernatant was concentrated via Amicon (MWCO = 50 kDa, Merck Millipore) to 500 μL. A total of 16 μL were used for an SDS-PAGE and sent for Mass spectrometry.

Fluorescence Time-Lapse Microscopy

For microscopy, 3 μL of stained cells were pipetted on a 0.3% agarose pad consisting of agarose dissolved in CAB medium supplemented with 10 μg/mL uracil. Phase-contrast and fluorescence images were captured every 30 min for 16 h at 100× magnification using a 100×/1.4 oil plan-apochromatic objective lens Ph 3, in phase contrast and fluorescence mode, using a Zeiss Axio Observer 2.1 microscope equipped with a heated XL-5 2000 Incubator while running VisiVIEW® software. Images were taken with the PCO Edge sCMOS Camera (PCO) with 50 ms exposure time for the phase contrast images and 500 ms for the GFP images. Images were analyzed using ImageJ, Fiji (Schindelin et al., 2012).

RESULTS

Whole Cell *in situ* Electron Cryo-Tomography Captures Cell–Cell Bridges Between Two *H. volcanii* Cells

To investigate the structure of the cell–cell bridges in *H. volcanii*, whole-cell electron cryoET was used. CryoET offers the possibility to image cells in their native environment in a near-native frozen-hydrated state to macromolecular resolutions. Cryomicrographs of vitrified *H. volcanii* cells grown in liquid medium were acquired. The initial tomograms showed archaellated cells with a possible storage granule as well as ribosomes in the cytoplasm (**Figure 1**). All detected cells were enveloped by a continuous 2D crystalline and proteinaceous S-layer over the membrane (**Figure 1**). In *H. volcanii*, the S-layer consist of many copies of one highly glycosylated protein that is secreted and lipid anchored to the membrane (Kessel et al., 1988; Sumper et al., 1990). The S-layer protein self-assembles to a 2D-lattice around the cell acting as a molecular sieve, supposed to be involved in cell recognition and cell shape maintenance (Sára and Sleytr, 2000; Sleytr et al., 2014). Strikingly, S-layer proteins could be detected, arranged in a hexagonal lattice around the cell similarly as reported in an early study (**Figure 1B**; Kessel et al., 1988). Upon closer investigation of a subtomogram slice, the dome shape morphology formed by S-layer proteins can be identified (**Figure 1C**; Kessel et al., 1988). The thickness of the S-layer was determined by measuring the distance from the membrane to the S-layer protein. The average thickness was determined to 20.4 ± 2.7 nm (**Supplementary Table 1**).

Interestingly, cryoET allowed the observation of several cells in a hemifusion state connected via cell–cell bridges (**Figure 2**, upper panels and **Supplementary Figure 1**). In total, out of 280 collected tilt series 20 tilt series of cell–cell bridges were acquired with a magnification sufficient to focus on the intercellular bridges (**Figure 2**, lower panels). As well as cell–cell bridges between intact cells (**Figure 2**, left panels), we observed cell bridges between intact and broken cells (**Figure 2**, middle panels) and disrupted cell bridges. Probably, these bridges ruptured during the cell isolation or during the blotting procedure. A representative tilt series is shown in **Supplementary Movie 1**.

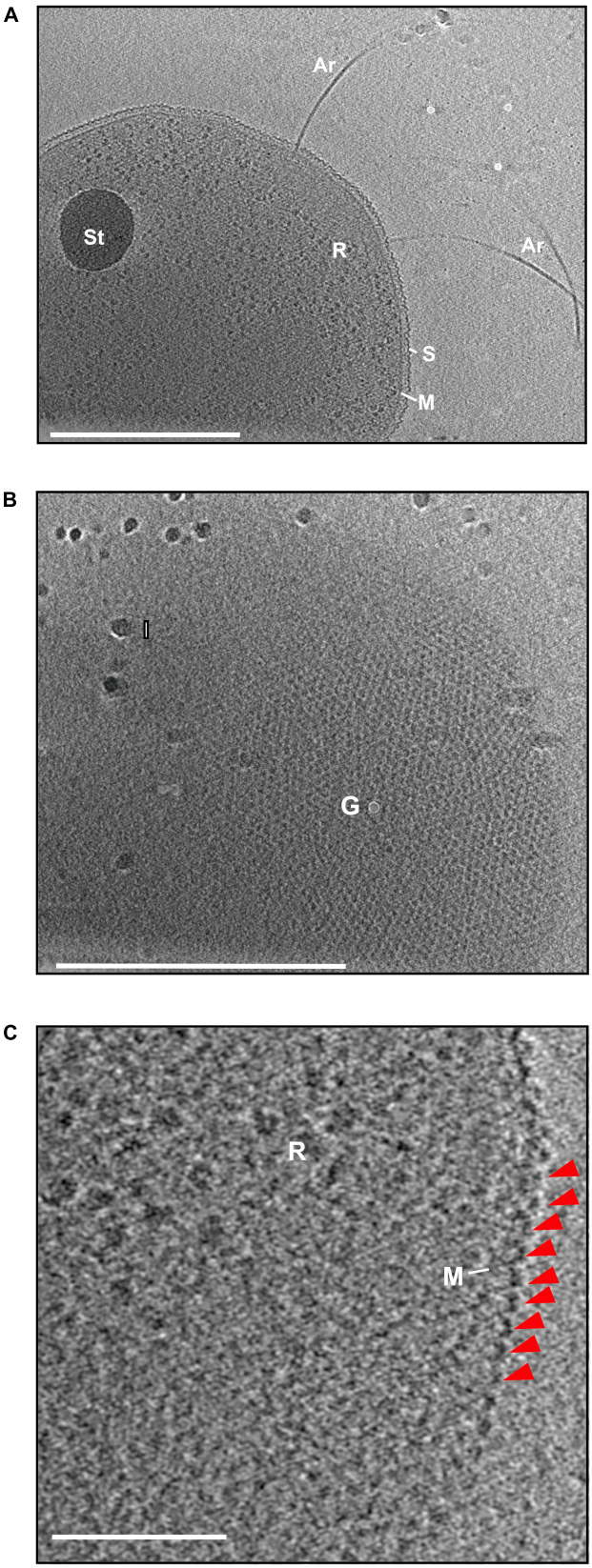

FIGURE 1 | Continued

FIGURE 1 | Electron cryo microscopy and subtomogram slices of *H. volcanii*. **(A)** A slice through the reconstructed tomogram of *H. volcanii*. The subtomographic slice reveals the cells filled with ribosomes (R) and a possible storage granule (St). The cells are enveloped by the cytoplasmic membrane (M) and a S-layer (S). From the cells, the archaellar motility system, the archaellum, extends (Ar). Scale bar is 500 nm. **(B)** Extracted subtomographic slice, showing the top view of the cell. The cell body is covered by the hexagonal arranged S-layer lattice. Gold fiducial (G) and ice crystal (I) contaminations are indicated. Scale bar is 500 nm. **(C)** A magnified tomographic slice from **(A)** showing the characteristic dome-like shape the arranged S-layer protein indicated by a red arrow. Scale bar is 100 nm.

We measured the widths and lengths of cell–cell bridges. The width was measured over the length of the cell–cell bridge and average width of each cell–cell bridge was determined (**Figure 3** and **Supplementary Table 1**). For determination of the length, only the cell–cell bridges were considered that connected two cells as shown in **Figure 2** (left and middle panel). The width varied from 57 to 162 nm and the length varied from 253 to 2,144 nm (**Figure 3** and **Supplementary Table 1**). The scatter plot and histogram (**Figure 3**) shows that the majority of cell–cell bridges have a width up to 100 nm with a length of 1–1.2 μm indicating that cells might need to be within ∼1.2 μm for the formation of cell–cell bridges to occur. No relation between length and diameter could be detected.

Cell–Cell Bridges Are Surrounded by a Continuous S-Layer and Connect the Cytoplasms of Two Cells

Closer investigation of the cell–cell bridges showed that these bridges connected the cytoplasms of the two cells. The connected cytoplasm was surrounded by a continuous cytoplasmic membrane and a continuous S-layer (**Figure 4**). Since the cytoplasms of the two cells are connected, this would allow exchange of cytoplasmic materials between two cells. Indeed, we saw high molecular mass complexes consistent with the size, shape, and density of ribosomes within the tubular cell–cell bridges, suggesting that high molecular weight complexes are exchanged between mating cells (**Figure 4** and **Supplementary Movie 1**). Next to the ribosomes also unknown thin filamentous helical structures of 199 ± 18 nm long and 9.0 ± 2.3 nm wide (**Figure 4B** and **Supplementary Movie 1**) were observed in the one of the analyzed cell–cell bridge. The function and the proteins that form the thin filamentous helical structures are unclear although we speculate that they may be cytomotive filaments to drive cytoplasmic exchange.

In vivo Observation of the Formation of an Intercellular *H. volcanii* Cell–Cell Bridge

The tomograms showed that intercellular bridges are encapsulated by an S-layer. To follow the formation of a cell–cell bridge using time-lapse fluorescence microscopy, the cells were incubated with the Alexa Fluor 488 NHS Ester and the cells were followed over a period of 16 h. As expected, the cells were mainly fluorescently labeled on the outside. Comparison

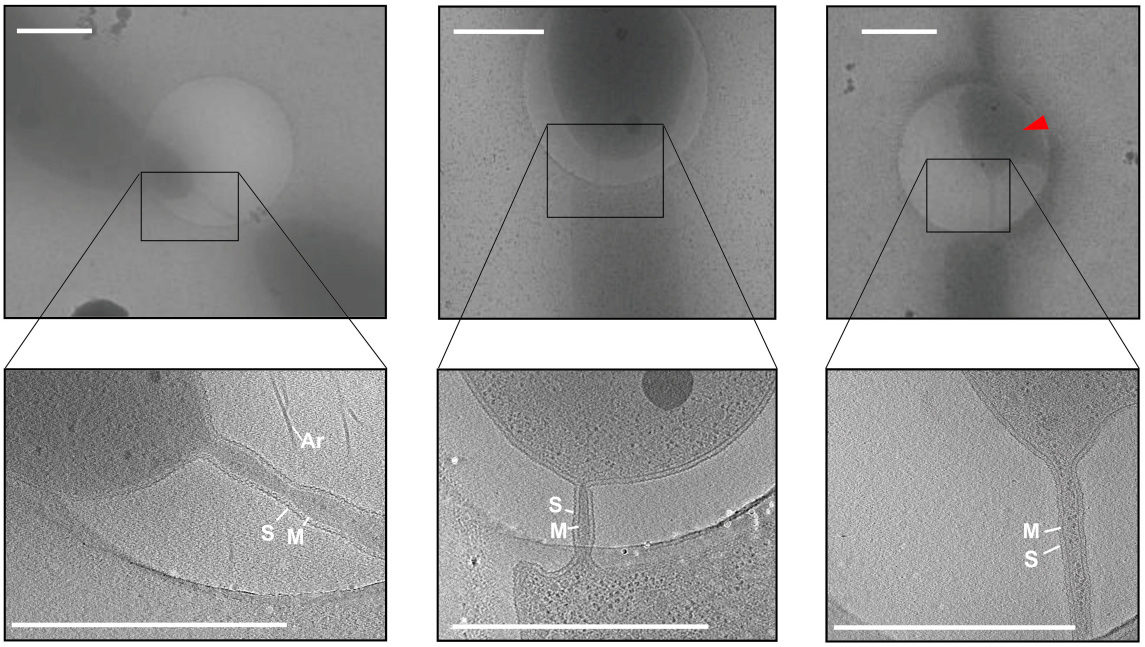

FIGURE 2 | Electron cryo microscopy and tomographic slices of cell–cell bridges in *H. volcanii*. Low magnification cryo micrographs of cell–cell bridges targeted for cryoET (upper panels) with the corresponding tomographic slice from a reconstructed tilt series (lower panels). The electron cryo micrographs as well and the corresponding slice through tomograms depict the variety in shape, length and width of the cell–cell bridges. The right panel shows a partially ruptured cell indicated by a red arrow. Scale bars are 1 μm. The cytoplasmic membrane (M), the S-layer (S), and archaella (Ar) are indicated.

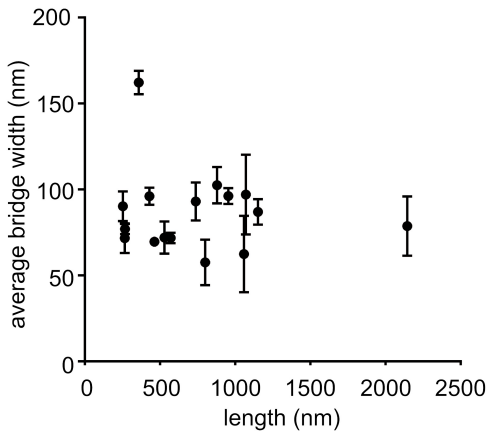

FIGURE 3 | Determination of length and width of cell–cell bridges. Scatter plot of length against the corresponding average width of cell–cell bridges. Six measurements of width per bridge were taken and average width with corresponding error were determined. Only cell–cell bridges were considered that connected two cells together (n = 16).

of the proteins which were labeled with the fluorescent probe in the total cell extract with isolated S-layers showed that, next to the S-layer protein, also several other proteins were labeled (**Supplementary Figure 2**). Several experiments were conducted where over 16 h every 30 min fluorescent and phase contrast images were acquired. In one of these experiments, the formation of a cell-bridge was observed. Notably, after 5 h of incubation, one thin fluorescent connection between two cells was detected that can be identified as a *de novo* formed cell–cell bridge (**Figure 5** and **Supplementary Movie 2**). The time lapse movie shows fluorescent cells with increasing cell size due to an unknown cell division defect where a fluorescent septum is formed between two adjacent cells which do not separate. This is sometimes observed during these experiments and is most likely unrelated to the observed cell–cell bridge. Between the 2:30 and 3:00 h time points a full cell–cell bridge is formed. Remarkably, the cell–cell bridge is formed between two cells at 1.5 μm distance without any initial direct contact, suggesting that cell–cell bridge formation is an active process. The analysis of CryoET data showed that shortly after cell–cell bridge formation the cytoplasms are most likely connected providing a connection between two cells and possibly allowing an exchange between two cells. It was not possible to determine whether the cell–cell bridge is formed from one or from both cells. After 7.5 h, the length of the cell–cell bridge is decreasing indicating a contraction to bring both cells in close proximity (**Figure 5**). The cell–cell bridge was maximally 1.5 μm long, growing shorter and thicker over time. Unfortunately, the *in vivo* formation of only one cell–cell bridge could be observed. However, this is the first time that the formation of a cell–cell bridge was observed in real time.

DISCUSSION

Mechanisms of gene transfer are diverse in Archaea (Meile et al., 1990; Schleper et al., 1995; Prangishvili et al., 1998; Bertani, 1999;

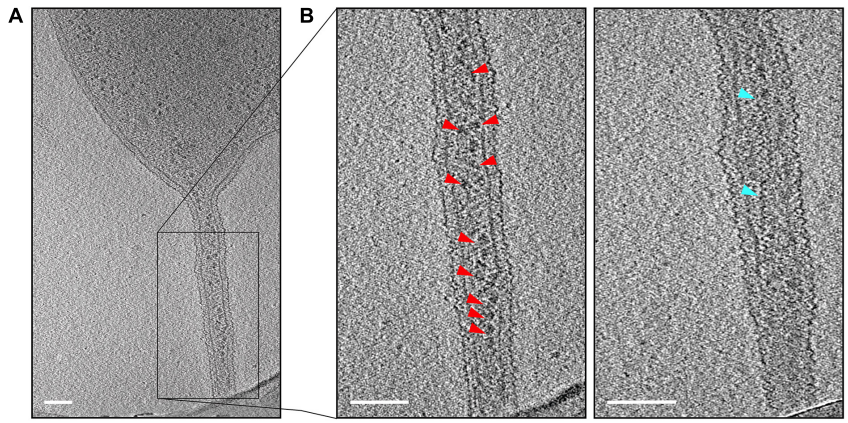

FIGURE 4 | Detection of macromolecular complexes in cell–cell bridges. **(A)** A micrograph of a targeted cell–cell bridge shows the presence of ribosomes in the cell–cell bridge (as indicated by red arrows). **(B)** The left panel shows the magnified tomographic slice of the cell–cell bridge and shows the ribosomes arranged in a chain-like manner (as indicated by red arrows). The right panel shows another slice of the selected cell–cell bridge showing a long filamentous structure inside the cell–cell bridge (as indicated by blue arrows). Scale bars are 100 nm.

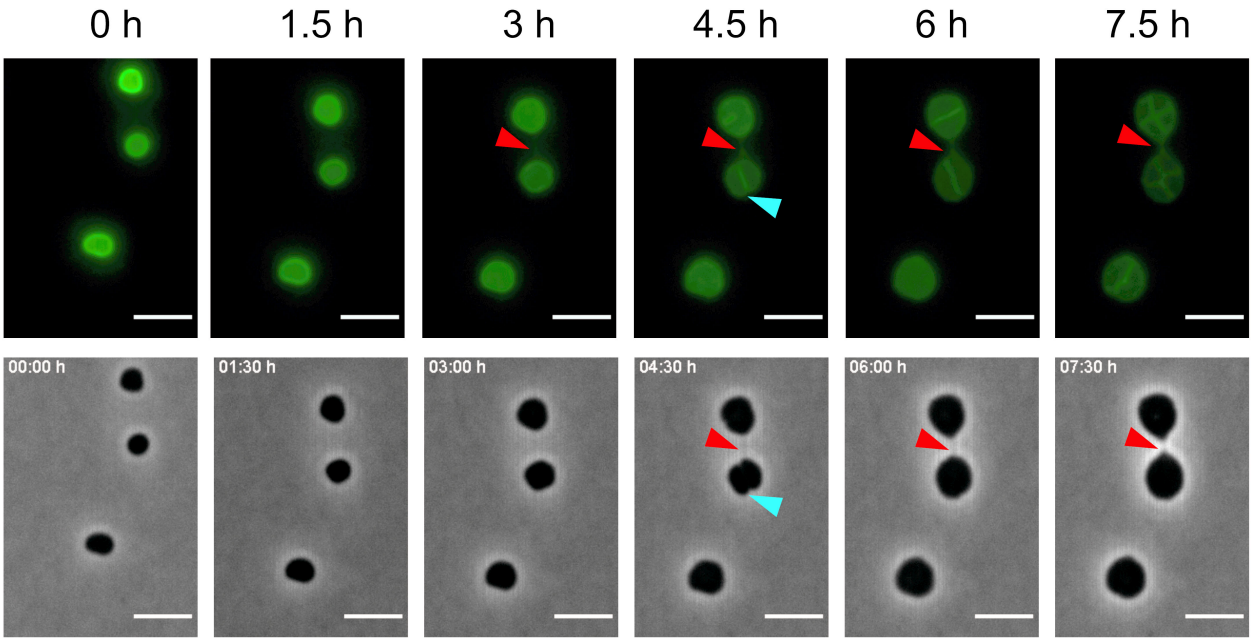

FIGURE 5 | Formation of a cell–cell bridge followed by fluorescence microscopy. Time-lapse fluorescence images of AlexaFluor488 labeled *H. volcanii* cells with the corresponding phase-contrast image. The fluorescence signal for the cell–cell bridge can be detected after 5 h and is indicated by a red arrow. In phase contrast, the cell–cell bridge can be detected after 7 h. Blue arrows indicate the septum formed between the cells due to a cell division defect. Scale bars are 4 μm.

Ajon et al., 2011; Allers, 2011; Naor et al., 2012; van Wolferen et al., 2013, 2020). In *H. volcanii* genetic transfer occurs in a bidirectional manner upon fusion (Mevarech and Werczberger, 1985; Rosenshine et al., 1989; Naor and Gophna, 2013) and it was proposed that the formation of cell–cell bridges may precede fusion as an intermediate state (Rosenshine et al., 1989; Naor and Gophna, 2013).

Whole-cell cryoET enabled preservation and the study of cells in this intermediate bridged state, while time-lapse fluorescence microscopy allowed for the observation of the formation of cell–cell bridges in real-time. Despite the high salinity of the cell cytoplasm and the medium, electron cryo-tomograms gave a high resolution snapshot of the features of the cell–cell bridges in *H. volcanii*. However, only a limited number of cell–cell bridges could be studied. In contrast to the cell–cell bridges observed by Mevarech and Rosenshine on solid media, bridge formation and fusion events were recorded in liquid media, but in liquid media, these events occur most likely much less frequently than

on solid media (Rosenshine et al., 1989). Furthermore, more cell–cell bridges would probably have been observed in a medium containing a higher salt concentration, as mating efficiency was shown to be higher at high salt concentrations (3.4 M NaCl), which is most likely caused by an altered S-layer glycosylation (Guan et al., 2012; Shalev et al., 2017). Since previous studies in *Halobacterium salinarum* showed that higher salt concentrations reduced the contrast of electron micrographs (Bollschweiler et al., 2017), images were obtained from cells grown in a medium containing 2.4 M NaCl where optimal growth was still observed.

Time-lapse fluorescence microscopy allowed for the observation of the *de novo* formation of a cell–cell bridge. This showed that cells are able to bridge the distance by the formation of a cell–cell bridge reaching to the adherent cell. The time-lapse fluorescence microscopy showed a cell–cell bridge that was formed over a distance of 1.5 μm whereas the cryoET showed that most cell-bridges were shorter than 1–1.2 μm, which demonstrates that cell-bridges with a length of ∼1 μm can be easily formed. Full cell–cell bridge formation was observed within 0.5 h, suggesting it is a relatively fast process (see **Supplementary Movie 2** between 2:30 and 3:00 h). Indeed, a recent transcriptomic study showed that mating impacts genes involved in cell division and glycosylation. Strikingly, increased expression was detected for selfish genetic elements, restriction-modification system and CRISPR-Cas. These changes were detected in the first hours after transfer to a filter paper, indicating that mating efficiency is probably the highest 4–8 h after cell contact (Makkay et al., 2020). Since adherence must be the first step before fusion, cells may initially form an S-layer covered protrusion that detects the adherent cell and initiates formation of the cell–cell bridge. Indeed, glycosylation of the S-layer is crucial in intraspecies mating efficiency (Shalev et al., 2017). Significantly fewer fusion events were observed when neither tetra- nor pentasaccharides decorated the S-layer protein (Shalev et al., 2017). In *Sulfolobales*, N-glycosylation of UV-inducible pili is also crucial for species-specific UV-induced aggregation. Addition of different sugars to the medium leads to decreased aggregation formation and ensuing reduced DNA exchange for DNA repair (van Wolferen et al., 2020). Similar to *Sulfolobales*, the N-glycan of a cell might be detected by surface-expressed receptor proteins for cell–cell recognition prior to cell–cell bridge formation. In addition, in *P. furiosus*, cell–cell contacts were shown to be mediated by bundles of glycosylated archaella (Näther et al., 2006).

All cell–cell bridges that were detected contained a connected S-layer and cytoplasm suggesting that the fusion of the cytoplasms occurs very shortly after the cell–cell bridge is formed. Time-lapse fluorescence microscopy indicated that the cell–cell bridge may shorten and widen for subsequent fusion of two cells (**Figure 5** and **Supplementary Movie 2**). The electron cryo-tomograms revealed a variety in the size of cell–cell bridges possibly due to the different fusion states that were detected. Upon closer investigation of the cell–cell bridges, ribosomes and other complexes among which thin filamentous helical structures were detected indicating an exchange of cytoplasmic components.

Cell–cell bridges (nanotubes) have also been identified between members of bacterial species and also connect the cytoplasms of neighboring cells, but still little is known about how they are formed (Dubey and Ben-Yehuda, 2011; Baidya et al., 2018). In Eukarya, cell fusion is a common mechanism, where gametes, myoblasts, or vesicles fuse to a partner or host cell. Fusion events are mostly mediated via fusogens (SNARE proteins) or fusexins in eukaryotic cells (Hernández and Podbilewicz, 2017; Segev et al., 2018). By a controlled re-organization/folding of the fusogens or fusexins in the membranes of the mating cells, the high energy barrier to cell–cell fusion can be overcome (Segev et al., 2018). Although two DedA-like proteins related to the SNARE-associated Tvp38 proteins in eukaryotes have been identified in *H. volcanii*, their role in the formation of cell–cell bridges remains unclear (Makkay et al., 2020). Also the role and identity of the thin filamentous helical structures observed in the cell–cell-bridges remains unknown. Here we have shown that *H. volcanii* can form cell–cell bridges which contain a continuous cytoplasm through which large molecular complexes like ribosomes can be exchanged. These structures might be further investigated by subtomogram averaging to elucidate the molecules involved, thus helping to understand their formation and role in the cell–cell bridges. The formation of a cell–cell bridge was observed between two cells ∼1.5 μm apart, suggesting this is an active process. These observations raise several new questions that should be addressed in future studies: How are these cell–cell bridges formed? Do these cell–cell bridges grow from one or from both cells? How do the cell–cell bridges fuse, and which proteins are required for the formation of the cell–cell bridges?

DATA AVAILABILITY STATEMENT

The original contributions presented in the study are included in the article/**Supplementary Material**, further inquiries can be directed to the corresponding author/s.

AUTHOR CONTRIBUTIONS

SS, PN, MB, and S-VA designed the research. SS performed the cryoET with technical help from Florian Rossmann (FR). SS, S-VA, and MB analyzed the tomograms, designed the figures, and wrote the manuscript. HW and PN performed the fluorescence microscopy. HW, PN, SS, and S-VA analyzed the fluorescence microscopy data and designed the figures. All authors read and reviewed the manuscript.

FUNDING

The article processing charge was funded by the University of Freiburg in the funding program Open Access Publishing. SS was supported by the Deutsche Forschungsgemeinschaft (German Research Foundation) under project no. 403222702-SFB 1381 and from the European Union's Horizon 2020 Research and

Innovation Program under grant agreement no. 686647. Mass spectrometry was performed with the help of the lab of Matthias Boll [supported by a grant from the German Research Foundation (INST 39/995-1 FUGG)].

ACKNOWLEDGMENTS

We thank Florian Rossmann (FR) and Paul Simpson for technical assistance with imaging *H. volcanii* for CryoET in the Imperial College Centre for Structural Biology Electron Microscopy Facility.

SUPPLEMENTARY MATERIAL

The Supplementary Material for this article can be found online at: https://www.frontiersin.org/articles/10.3389/fmicb.2020.612239/full#supplementary-material

REFERENCES

Ajon, M., Fröls, S., van Wolferen, M., Stoecker, K., Teichmann, D., Driessen, A. J. M. M., et al. (2011). UV-inducible DNA exchange in hyperthermophilic archaea mediated by type IV pili. *Mol. Microbiol.* 82, 807–817. doi: 10.1111/j.1365-2958.2011.07861.x

Allers, T. (2011). Swapping genes to survive - a new role for archaeal type IV pili. *Mol. Microbiol.* 82, 789–791. doi: 10.1111/j.1365-2958.2011.07860.x

Allers, T., Ngo, H. P., Mevarech, M., and Lloyd, R. G. (2004). Development of additional selectable markers for the halophilic archaeon *Haloferax volcanii* based on the leuB and trpA genes. *Appl. Environ. Microbiol.* 70, 943–953. doi: 10.1128/AEM.70.2.943-953.2004

Amat, F., Moussavi, F., Comolli, L. R., Elidan, G., Downing, K. H., and Horowitz, M. (2008). Markov random field based automatic image alignment for electron tomography. *J. Struct. Biol.* 161, 260–275. doi: 10.1016/j.jsb.2007.07.007

Baidya, A. K., Bhattacharya, S., Dubey, G. P., Mamou, G., and Ben-Yehuda, S. (2018). Bacterial nanotubes: a conduit for intercellular molecular trade. *Curr. Opin. Microbiol.* 42, 1–6. doi: 10.1016/j.mib.2017.08.006

Bertani, G. (1999). Transduction-like gene transfer in the methanogen *Methanococcus voltae*. *J. Bacteriol.* 181, 2992–3002. doi: 10.1128/jb.181.10.2992-3002.1999

Bollschweiler, D., Schaffer, M., Lawrence, C. M., and Engelhardt, H. (2017). Cryo-electron microscopy of an extremely halophilic microbe: technical aspects. *Extremophiles* 21, 393–398. doi: 10.1007/s00792-016-0912-0

Carragher, B., Kisseberth, N., Kriegman, D., Milligan, R. A., Potter, C. S., Pulokas, J., et al. (2000). Leginon: an automated system for acquisition of images from vitreous ice specimens. *J. Struct. Biol.* 132, 33–45. doi: 10.1006/jsbi.2000.4314

Comolli, L. R., and Banfield, J. F. (2014). Inter-species interconnections in acid mine drainage microbial communities. *Front. Microbiol.* 5:367. doi: 10.3389/fmicb.2014.00367

Cuadros-Orellana, S., Martin-Cuadrado, A. B., Legault, B., D'Auria, G., Zhaxybayeva, O., Papke, R. T., et al. (2007). Genomic plasticity in prokaryotes: the case of the square haloarchaeon. *ISME J.* 1, 235–245. doi: 10.1038/ismej.2007.35

Dubey, G. P., and Ben-Yehuda, S. (2011). Intercellular nanotubes mediate bacterial communication. *Cell* 144, 590–600. doi: 10.1016/j.cell.2011.01.015

Duggin, I. G., Aylett, C. H. S. S., Walsh, J. C., Michie, K. A., Wang, Q., Turnbull, L., et al. (2015). CetZ tubulin-like proteins control archaeal cell shape. *Nature* 519, 362–365. doi: 10.1038/nature13983

Eiserling, F., Pushkin, A., Gingery, M., and Bertani, G. (1999). Bacteriophage-like particles associated with the gene transfer agent of *Methanococcus voltae* PS. *J. Gen. Virol.* 80, 3305–3308. doi: 10.1099/0022-1317-80-12-3305

Esquivel, R. N., and Pohlschroder, M. (2014). A conserved type IV pilin signal peptide H-domain is critical for the post-translational regulation of flagella-dependent motility. *Mol. Microbiol.* 93, 494–504. doi: 10.1111/mmi.12673

Fröls, S., Ajon, M., Wagner, M., Teichmann, D., Zolghadr, B., Folea, M., et al. (2008). UV-inducible cellular aggregation of the hyperthermophilic archaeon *Sulfolobus solfataricus* is mediated by pili formation. *Mol. Microbiol.* 70, 938–952. doi: 10.1111/j.1365-2958.2008.06459.x

Fröls, S., White, M. F., and Schleper, C. (2009). Reactions to UV damage in the model archaeon *Sulfolobus solfataricus*. *Biochem. Soc. Trans.* 37, 36–41. doi: 10.1042/BST0370036

Guan, Z., Naparstek, S., Calo, D., and Eichler, J. (2012). Protein glycosylation as an adaptive response in Archaea: growth at different salt concentrations leads to alterations in *Haloferax volcanii* S-layer glycoprotein N-glycosylation. *Environ. Microbiol.* 14, 743–753. doi: 10.1111/j.1462-2920.2011.02625.x

Hernández, J. M., and Podbilewicz, B. (2017). The hallmarks of cell-cell fusion. *Development* 144, 4481–4495. doi: 10.1242/dev.155523

Kessel, M., Wildhaber, I., Cohen, S., and Baumeister, W. (1988). Three-dimensional structure of the regular surface glycoprotein layer of *Halobacterium volcanii* from the Dead Sea. *EMBO J.* 7, 1549–1554. doi: 10.1002/j.1460-2075.1988.tb02974.x

Kremer, J. R., Mastronarde, D. N., and McIntosh, J. R. (1996). Computer visualization of three-dimensional image data using IMOD. *J. Struct. Biol.* 116, 71–76. doi: 10.1006/jsbi.1996.0013

Kuwabara, T., Minaba, M., Iwayama, Y., Inouye, I., Nakashima, M., Marumo, K., et al. (2005). *Thermococcus coalescens* sp. nov., a cell-fusing hyperthermophilic archaeon from Suiyo Seamount. *Int. J. Syst. Evol. Microbiol.* 55, 2507–2514. doi: 10.1099/ijs.0.63432-0

Lang, A. S., Zhaxybayeva, O., and Beatty, J. T. (2012). Gene transfer agents: phage-like elements of genetic exchange. *Nat. Rev. Microbiol.* 10, 472–482. doi: 10.1038/nrmicro2802

Lipscomb, G. L., Stirrett, K., Schut, G. J., Yang, F., Jenney, F. E., Scott, R. A., et al. (2011). Natural competence in the hyperthermophilic archaeon *Pyrococcus furiosus* facilitates genetic manipulation: construction of markerless deletions of genes encoding the two cytoplasmic hydrogenases. *Appl. Environ. Microbiol.* 77, 2232–2238. doi: 10.1128/aem.02624-10

Makkay, A., Louyakis, A., Ram-Mohan, N., Gophna, U., Gogarten, J. P., and Papke, R. T. (2020). Insights into gene expression changes under conditions that facilitate horizontal gene transfer (mating) of a model Archaeon. *bioRxiv [Preprint]* doi: 10.1101/2020.07.06.189845

Mastronarde, D. N. (1997). Dual-axis tomography: an approach with alignment methods that preserve resolution. *J. Struct. Biol.* 120, 343–352. doi: 10.1006/jsbi.1997.3919

Meile, L., Abendschein, P., and Leisinger, T. (1990). Transduction in the archaebacterium *Methanobacterium thermoautotrophicum* Marburg. *J. Bacteriol.* 172, 3507–3508. doi: 10.1128/jb.172.6.3507-3508.1990

Mevarech, M., and Werczberger, R. (1985). Genetic transfer in *Halobacterium volcanii*. *J. Bacteriol.* 162, 461–462. doi: 10.1128/jb.162.1.461-462.1985

Mizuno, C. M., Prajapati, B., Lucas-Staat, S., Sime-Ngando, T., Forterre, P., Bamford, D. H., et al. (2019). Novel haloarchaeal viruses from Lake Retba infecting *Haloferax* and *Halorubrum* species. *Environ. Microbiol.* 21, 2129–2147. doi: 10.1111/1462-2920.14604

Mullakhanbhai, M. F., and Larsen, H. (1975). *Halobacterium volcanii* spec. nov., a Dead Sea halobacterium with a moderate salt requirement. *Arch. Microbiol.* 104, 207–214. doi: 10.1007/BF00447326

Naor, A., and Gophna, U. (2013). Cell fusion and hybrids in Archaea: prospects for genome shuffling and accelerated strain development for biotechnology. *Bioengineered* 4, 126–129. doi: 10.4161/bioe.22649

Naor, A., Lapierre, P., Mevarech, M., Papke, R. T., and Gophna, U. (2012). Report low species barriers in halophilic Archaea and the formation of recombinant hybrids. *Curr. Biol.* 22, 1444–1448. doi: 10.1016/j.cub.2012.05.056

Näther, D. J., Rachel, R., Wanner, G., and Wirth, R. (2006). Flagella of *Pyrococcus furiosus*: multifunctional organelles, made for swimming, adhesion to various surfaces, and cell-cell contacts. *J. Bacteriol.* 188, 6915–6923. doi: 10.1128/jb.00527-06

Prangishvili, D., Albers, S. V., Holz, I., Arnold, H. P., Stedman, K., Klein, T., et al. (1998). Conjugation in archaea: frequent occurrence of conjugative plasmids in Sulfolobus. *Plasmid* 40, 190–202. doi: 10.1006/plas.1998.1363

Quemin, E. R. J., Chlanda, P., Sachse, M., Forterre, P., Prangishvili, D., and Krupovic, M. (2016). Eukaryotic-like virus budding in archaea. *mBio* 7:e01439-16.

Rosenshine, I., Tchelet, R., and Mevarech, M. (1989). The mechanism of DNA transfer in the mating system of an archaebacterium. *Science* 245, 1387–1389. doi: 10.1126/science.2818746

Sára, M., and Sleytr, U. B. (2000). S-layer proteins. *J. Bacteriol.* 182, 859–868. doi: 10.1128/JB.182.4.859-868.2000

Sato, T., Fukui, T., Atomi, H., and Imanaka, T. (2005). Improved and versatile transformation system allowing multiple genetic manipulations of the hyperthermophilic archaeon *Thermococcus kodakaraensis*. *Appl. Environ. Microbiol.* 71, 3889–3899. doi: 10.1128/AEM.71.7.3889-3899.2005

Schindelin, J., Arganda-Carreras, I., Frise, E., Kaynig, V., Longair, M., Pietzsch, T., et al. (2012). Fiji: an open-source platform for biological-image analysis. *Nat. Methods* 9, 676–682. doi: 10.1038/nmeth.2019

Schleper, C., Holz, I., Janekovic, D., Murphy, J., and Zillig, W. (1995). A multicopy plasmid of the extremely thermophilic archaeon *Sulfolobus* effects its transfer to recipients by mating. *J. Bacteriol.* 177, 4417–4426. doi: 10.1128/jb.177.15.4417-4426.1995

Schleper, C., Kubo, K., and Zillig, W. (1992). The particle SSV1 from the extremely thermophilic archaeon *Sulfolobus* is a virus: demonstration of infectivity and of transfection with viral DNA. *Proc. Natl. Acad. Sci. U.S.A.* 89, 7645–7649. doi: 10.1073/pnas.89.16.7645

Segev, N., Avinoam, O., and Podbilewicz, B. (2018). Fusogens. *Curr. Biol.* 28, R378–R380. doi: 10.1016/j.cub.2018.01.024

Shalev, Y., Turgeman-Grott, I., Tamir, A., Eichler, J., and Gophna, U. (2017). Cell surface glycosylation is required for efficient mating of *Haloferax volcanii*. *Front. Microbiol.* 8:1253. doi: 10.3389/fmicb.2017.01253

Sleytr, U. B., Schuster, B., Egelseer, E.-M., and Pum, D. (2014). S-layers: principles and applications. *FEMS Microbiol. Rev.* 38, 823–864.

Soler, N., Marguet, E., Verbavatz, J. M., and Forterre, P. (2008). Virus-like vesicles and extracellular DNA produced by hyperthermophilic archaea of the order *Thermococcales*. *Res. Microbiol.* 159, 390–399. doi: 10.1016/j.resmic.2008.04.015

Stedman, K. M., She, Q., Phan, H., Holz, I., Singh, H., Prangishvili, D., et al. (2000). pING family of conjugative plasmids from the extremely thermophilic archaeon *Sulfolobus islandicus*: insights into recombination and conjugation in Crenarchaeota. *J. Bacteriol.* 182, 7014–7020. doi: 10.1128/JB.182.24.7014-7020.2000

Sumper, M., Berg, E., Mengele, R., and Strobel, I. (1990). Primary structure and glycosylation of the S-layer protein of *Haloferax volcanii*. *J. Bacteriol.* 172, 7111–7118. doi: 10.1128/jb.172.12.7111-7118.1990

Tschitschko, B., Erdmann, S., DeMaere, M. Z., Roux, S., Panwar, P., Allen, M. A., et al. (2018). Genomic variation and biogeography of Antarctic haloarchaea. *Microbiome* 6:113.

Turgeman-Grott, I., Joseph, S., Marton, S., Eizenshtein, K., Naor, A., Soucy, S. M., et al. (2019). Pervasive acquisition of CRISPR memory driven by inter-species mating of archaea can limit gene transfer and influence speciation. *Nat. Microbiol.* 4, 177–186. doi: 10.1038/s41564-018-0302-8

van Wolferen, M., Ajon, M., Driessen, A. J. M., and Albers, S.-V. (2013). Molecular analysis of the UV-inducible pili operon from *Sulfolobus acidocaldarius*. *Microbiologyopen* 2, 928–937. doi: 10.1002/mbo3.128

van Wolferen, M., Shajahan, A., Heinrich, K., Brenzinger, S., Black, I. M., Wagner, A., et al. (2020). Species-specific recognition of *Sulfolobales* mediated by UV-inducible pili and S-Layer glycosylation patterns. *mBio* 11:e03014-19.

Van Wolferen, M., Wagner, A., Van Der Does, C., and Albers, S. V. (2016). The archaeal Ced system imports DNA. *Proc. Natl. Acad. Sci. U.S.A.* 113, 2496–2501. doi: 10.1073/pnas.1513740113

Wagner, A., Whitaker, R. J., Krause, D. J., Heilers, J.-H., van Wolferen, M., van der Does, C., et al. (2017). Mechanisms of gene flow in archaea. *Nat. Rev. Microbiol.* 15, 492–501. doi: 10.1038/nrmicro.2017.41

Conflict of Interest: The authors declare that the research was conducted in the absence of any commercial or financial relationships that could be construed as a potential conflict of interest.